CTU Journal of Innovation and Sustainable Development
ISSN 2615-9422 | e-ISSN 2815-5602

DOI:10.22144/ctujoisd.2024.271

Compatibility and effect of capacity ratios between $Na_3V_2(PO_4)_3$ and hard carbon in highly concentrated sodium bis (fluorosulfonyl) imide electrolyte

Phuong Quy Chau[1], Liem Thanh Pham[1], Quan Dinh Nguyen[2], My Loan Phung Le[1,3], Man Van Tran[1,3], and Trung Thien Nguyen[4*]

[1]*Applied Physical Chemistry Laboratory, University of Science, VNU-HCMC, Viet Nam*

[2]*Biofuel and Biomass Research Laboratory, Faculty of Chemical Engineering, University of Technology, VNU-HCMC, Viet Nam*

[3]*Department of Physical Chemistry, Faculty of Chemistry, University of Science, VNU-HCMC, Viet Nam*

[4]*Central Laboratory for Analysis, University of Science, VNU-HCMC, Viet Nam*

**Corresponding author (ngttrung@hcmus.edu.vn)*

Article info.

Received 21 Aug 2023
Revised 14 Sep 2023
Accepted 18 Sep 2023

Keywords

High concentration electrolyte, matching up full cell, Sodium-ion batteries

ABSTRACT

From the standpoint of preserving the Earth's resources and ensuring the long-term viability of humanity, it is imperative to transition away from lithium-ion batteries. High-performance and safe sodium-ion batteries have recently emerged as promising advanced batteries for application in stationary energy storage, attributed to their low cost and abundance of sodium ion. We demonstrate the compatibility and effect of the negative-positive capacity ratio in full-cell $Na_3V_2(PO_4)_3$ and hard carbon in high-concentration electrolytes. Thanks to the excellent oxidation stability of the electrolyte, during 100 cycles, the full cell with a negative-positive capacity ratio of 1.1 demonstrated a consistent capacity of around 100 mAh g^{-1} with a capacity retention of 90.7%, whereas the full cell with a ratio of 1.0 showed a steady discharge capacity of roughly 90 mAh g^{-1} with a capacity retention of approaching 100% at a current density of C/5.

1. INTRODUCTION

Over the past few decades, one of promising energy sources that can be an alternative to lithium-ion batteries (LIBs) has been sodium-ion batteries (SIBs). On account of the similarity in properties between sodium and lithium, inexhaustible and widely contributed sodium resources, high energy density, and unexpensive costs, SIBs can be applied as an energy source in certain applications, such as stationary large-scale energy storage (Zheng et al., 2018; Ma et al., 2020). The large ionic radius of Na^+ motivated significant studies focusing on screening appropriate cathode materials as the host of Na^+, which steadily maintain high capacity and crystal structure during Na^+ insertion/extraction to ensure good cycling stability (Dou et al., 2023). A NASICON material, $Na_3V_2(PO_4)_3$ (NVP), with a three-dimensional structure and high Na^+ conductivity, has been one of the most prospective materials for SIBs and attracted interest in materials improvement (Shen et al., 2021; Li et al., 2023; Dou et al., 2023; Tran et al., 2023).

Recent advancements have been made in enhancing the properties of materials, specifically in locating anode materials that are compatible with advanced cathode materials. Thanks to its low cost, capacitive and structural stability, and eco-friendliness, hard carbon (HC) is a prominent candidate for this function. However, commercializing hard carbon-based SIBs has been challenging because of their

low initial coulombic efficiency (ICE). The low ICE caused by the irreversible sodium insertion is attributed to the sodium trapping process at defect sides in bulk HC (i.e., adatoms, dangling bonds, and so on) (Bommier et al., 2015; Nguyen & Duong, 2020), along with the continuous decomposition of electrolyte components to form a solid electrolyte interphase (SEI) on the anode surface. This irreversible process leads to a significant loss of active sodium coming from cathode and electrolytes. Similar to the prelithiation process in LIBs, presodiation has been considered one of the most effective treatments to counteract the energy loss caused by the limited sodium resource in cathode materials and the irreversible Na^+ insertion in HC structure. There are three categories of pre-treatment on HC electrode including chemical, electrochemical, and direct-contact presodiation (Moeez et al., 2019; Xie et al., 2021).

Besides advanced electrode strategies, electrolytes as the most vital components, which dictate the interfacial electrode properties and further affect cell performance, have been recently facilitated. Commonly used carbonate-based electrolytes suffer from forming an unstable, porous, and thick SEI layer on the anode surface. Alternatively, ether-based electrolytes have been considered outstanding electrolytes that produce a thin, dense, and uniform SEI layer as well as enhance cell cycling performance and lifespan. Hayley S. Hirsh's group showed that a minimal thickness, exceptional conformity, and uniform distribution of SEI was formed on HC anode in (1 M $NaBF_4$ in TEGDME) which enabled a superior cycling performance than that of HC in (1 M $NaPF_6$ in PC) electrolyte (Xie et al., 2021. A new class of electrolytes, known as high concentration electrolytes (HCEs), attracted the intensive attention of scientists as a high-safety and high-performance electrolyte (Yamada, 2020). Problems of flammable, leakage-vapor solvent, unstable SEI, metal dendritic growth, current collector corrosion, and so on that suppress cell performance and pose a risk of safety were solved, attributed to high salt concentrations and a minority of free solvent molecules in HCEs (Cao et al., 2016; Lee et al., 2017; Hirsh et al., 2021).

One of the critical factors in full cell design is the capacity ratio of the negative to the positive electrode (N/P ratio) since it has an enormous impact on the battery's energy density, cycle life, overcharge safety, and cost (Wu et al., 2009). Sodium plating, when being charged, is one of the electrochemical characteristics directly related to the N/P ratio. Cycling produces the accumulation of sodium plating, which is irreversible and causes capacity loss, mechanical swelling, as well as internal short-circuits (Hwang et al., 2017; Ilarduya et al., 2017; Song et al., 2023; Zhang et al., 2023). Although the influence of the N/P ratio on electrochemical reactions is a key factor in the performance of full cells, there are few practical investigations of the N/P ratio for sodium-ion batteries.

In this study, we investigated the compatibility of hard carbon as well as the influence of N/P ratios with different values (ranging from 0.8 to 1.2) on battery performance in full cell HC||NVP in highly concentrated NaFSI/DME electrolytes. By fixing the cathode electrode and adjusting the anode electrode mass loading, various N/P ratios can be attained.

2. MATERIALS AND METHOD

2.1. Preparation of electrolyte

Sodium bis(fluorosulfony)imide (NaFSI, Solvionic, > 99.7%) was dissolved in Ethylene glycol dimethyl ether (DME, Sigma Aldrich, > 99.9%) within various NaFSI/DME weight ratios, including 1:3, 1:2, 1:1, 2:1, and 2.5:1 to prepare HCEs. The NaFSI/DME used for cell testing was prepared by dissolving NaFSI in DME with a weight ratio of 2:1 (NaFSI/DME 2:1), and fluoroethylene carbonate (FEC, Sigma Aldrich, > 99%) 3 wt.% was added as the salt was completely dissolved in the solvent. An Argon filled glovebox (MBRAUN, Germany) was employed to prepare electrolyte with the content of both H_2O and O_2 less than 0.5 ppm.

2.2. Fabrication of electrodes

The cathode electrode was fabricated by depositing a mixture of $Na_3V_2(PO_4)_3$ (NVP, MTI, 99.9%), carbon black (Super P, Imerys) and poly(vinylidene fluoride) (PVdF, MTI) with a weight ratio of 80:15:5 in anhydrous N-methyl-2-pyrrolidone (NMP, Sigma Aldrich, > 99.0%) onto an aluminum foil. The electrodes were roll-pressed at room temperature and punched into circles with a diameter of 12 mm. Then, the electrodes were placed in a vacuum oven and dried at 110^{o}C for 12 hours. Mass loading of electrodes was controlled at 3–4 mg cm^{-2}.

The anode electrode was fabricated by casting a slurry comprising hard carbon (HC, Kurato, type 2, Japan), carbon conductive agent (Super P, Imerys) and binder (carboxymethyl cellulose, CMC)

dissolved in deionized water with a weight ratio of 90:5:5 onto a copper foil. The electrodes were roll-pressed at room temperature and punched into 14 mm – diameter circles. Then, the electrodes were placed in a vacuum oven and dried at 80°C for 12 hours

2.3. Materials characterizations

The morphology of NVP and HC electrodes was characterized by scanning electron microscopy (SEM, JSM IT200), with an EDS analysis. A D8 advance eco (Bruker, Germany) was employed to collect a X-ray diffraction (XRD) patterns using Cu Kα radiation (λ=1.5406 Å).

To evaluate the thermal stability of NaFSI/DME electrolytes at different temperature conditions, several milligrams of the materials were characterized by thermogravimetric analysis (TGA) on STA PT 1600 (Linseis, Germany), in an inert atmosphere (Argon) at room temperature (35 °C), and elevated temperature (55 °C) within 60 minutes.

2.4. Electrochemical characterizations

The electrochemical properties were evaluated by galvanostatic cycling using a Lanhe CT2001A (China). A CR2032 half-cell comprising NVP as a working electrode, sodium metal as a counter electrode, and a glass fiber separator (GF/C, Whatman) filled with 200 µL of electrolyte. The cell was tested at the voltage range from 2.5 to 3.7 V, and a current density of C/10 (1C = 117.6 mAh g^{-1}) in 100 cycles.

The half-cell Na||HC cells that were used HC electrode instead of NVP electrode were tested at the voltage range from 0.01 to 2.0 V, and a current density of 20 mA g^{-1} in 100 cycles. In the presodiation method, the electrodes were immersed in 1.0 M NaFSI in DME and simultaneously exposed to the sodium metal surface for 30 minutes prior to cell assembly.

Full-cell HC||NVP assembled with negative to positive (N/P) capacity ratios of 0.8, 0.9, 1.0, 1.1, and 1.2 were tested at the voltage range between 2.5 and 3.7 V, and a current density of C/5 (1C = 117.6 mAh g^{-1}) in 100 cycles. All cells were assembled in Ar-filled glovebox.

3. RESULTS AND DISCUSSION

The outstanding physicochemical properties, Al corrosion inhibition feature, and the compatibility of NVP cathodes in NaFSI/DME FEC 3 wt.% electrolyte were demonstrated in our previous report (Nguyen et al., 2023). To further highlight the superior thermal endurance, thermogravimetric analysis (TGA) was carried out at ambient temperature (35°C) and elevated temperature (55 °C). As shown in Figure 1, there was a significant weight loss in dilute concentration electrolytes (NaFSI/DME 1:3, 1:2, 1:1) caused by solvent evaporation. In contrast, there was only around 5% of total weight loss even at 55 °C in HCEs (NaFSI/DME 2:1, 2:5:1). This further proves the outstanding thermal stability of the high concentration electrolytes. Additionally, the superior cycling behavior of NVP electrode using NaFSI/DME (2:1) FEC 3 wt.% was depicted in Figure 2. Therefore, further investigation was conducted in this research pertaining to the compatibility of HC anode, as well as the compatibility of full-cell NVP and HC in highly concentrated electrolytes.

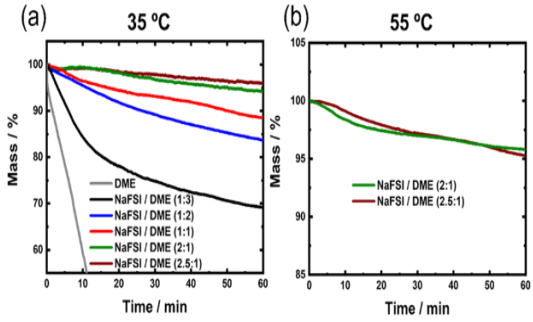

Figure 1. Thermal endurance of high concentration electrolytes NaFSI/DME

The structure of HC was characterized using XRD. Figure 3 (a) shows a typical XRD pattern of HC. XRD pattern exhibits a broad reflection at around 2θ = 22.8°, and 43.6°, corresponding to (002), and (100) planes of graphite, respectively, with rapidly decreasing intensity. The broad reflection is associated with the disordered graphitic sheet. Moreover, presodiation has been considered as an effective way to solve the irreversible sodium insertion as well as enhance low ICE of HC (Moeez et al., 2019; Xie et al., 2021). Scanning electron microscopy (SEM) and energy-dispersive X-ray spectroscopy (EDS) techniques were used to compare the morphology and elemental composition of pristine and presodiated HC electrodes. The results are presented in Figure 3 (b,c), Figure 4, and Figure 5. The morphology of the HC electrodes was unaffected by chemical presodiation, as shown in Figure 3 (b, c) and Figure 4. However, as evidenced by EDS results (Figure 5), presodiation has inserted a noticeable amount of

sodium, which was approximately 7% in atom (Table 1), whereas pristine HC consists only of carbon.

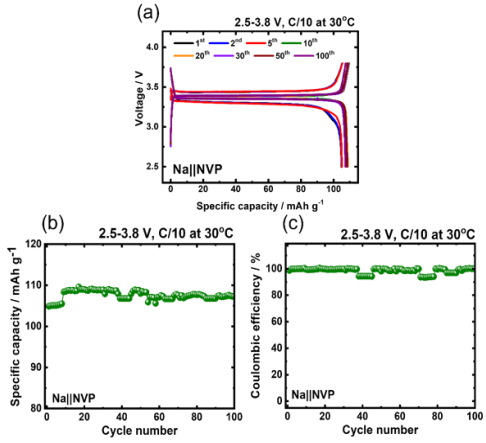

Figure 2. (a) Voltage profiles and (b, c) cycling performance of Na||NVP in NaFSI/DME (2:1) FEC 3 wt.%

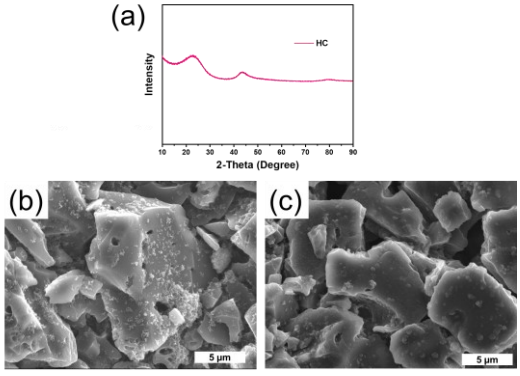

Figure 3. (a) XRD pattern of HC powder; SEM (b) pristine and (c) presodiated HC electrodes

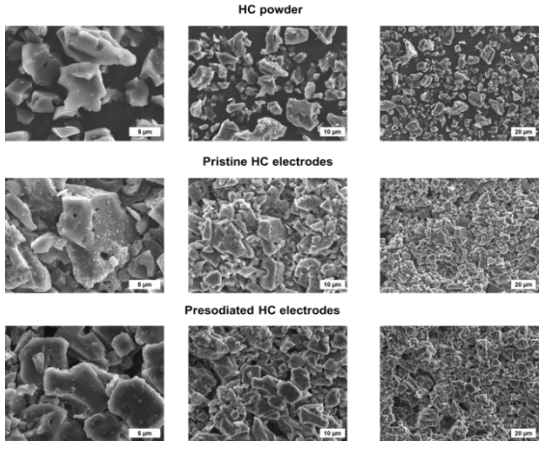

Figure 4. SEM images of HC powder, pristine HC electrodes, and presodiated HC electrodes

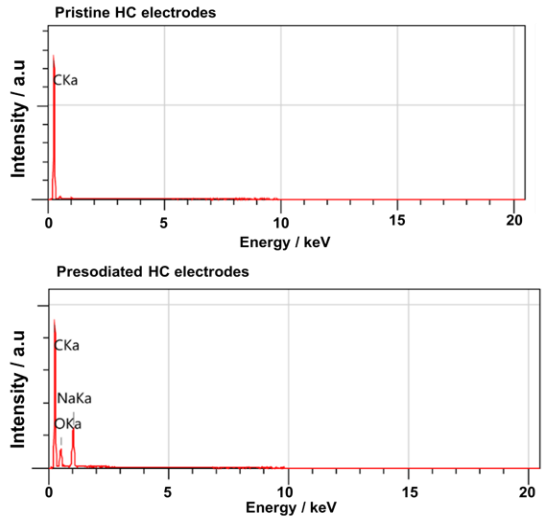

Figure 5. EDS spectrum of pristine HC electrodes, and presodiated HC electrodes

Table 1. Element components in pristine and presodiated HC electrodes

Sample	Atom%		
	C	Na	O
Pristine HC	100 ± 0.41	-	-
Presodiation HC	76.77 ± 0.41	7.35 ± 0.15	15.89 ± 0.35

The electrochemical performances of pristine and presodiated HC were analyzed by galvanostatic charge/discharge in voltage range of 0.01-2.0 V (1C = 200 mAh g^{-1}). As shown in Figure 6, for a pristine HC electrode, HCEs NaFSI/DME (2:1) FEC 3 wt.% displayed a higher discharge capacity of approximately 200 mAh g^{-1}, as compared to approximately 90 mAh g^{-1} of dilute electrolyte NaFSI/DME (1:3) FEC 3 wt.%. Figure 7 shows voltage profiles and cycling performance of HC electrodes with and without presodiation. The lower cut-off voltage was set at 0.01 V to avoid sodium plating. The voltage profiles of both HC electrodes with and without presodiation exhibited two distinguishable regions: a sloping-voltage region and a plateau-voltage region, indicative of underlying sodium ions storage mechanism within the HC anode. The sloping region, along with the observation of the rapid potential reduction at high voltage, was attributed to the adsorption effect of sodium ions in pores and defects of HC. The low-voltage plateau (< 0.2 V) could be assigned to the pore-filling process within the micro-nanocrystallites, which contributed to a large fraction of capacity (Huang et al., 2021). This result

indicated that the employment of NaFSI/DME (2:1), a highly concentrated electrolyte, provided an extra amount of active sodium ions, which could effectively enhance cycling capacity. As shown in Table 2, the ICE of pristine HC electrode was only 31%, corresponding to charge/discharge capacity of 66.3/215.6 mAh g^{-1}. It is noticeable that discharge capacity dramatically dropped to approximately 100 mAh g^{-1} in the second cycle, and gradually increased to about 200 mAh g^{-1} in subsequent cycles as shown in Figure 7 (a). According to several previous reports, such the limited ICE is ascribed to the formation of SEI by electrolyte decomposition and irreversible insertion of sodium ions into electrode structure, consuming an amount of active sodium (Pan et al., 2017; Xiao et al., 2018; Xie et al., 2019). In order to tackle this matter, the HC electrodes underwent presodiation with sodium metal. As a result, a presodiated HC electrode displayed an ICE of 97.5%, and an initial charge/discharge capacity of approximately 250 mAh g^{-1} was about 271% and 17% higher than that of pristine HC electrode. In addition, the capacity of presodiated HC remained steady at approximately 280 mAh g^{-1} during 100 cycles. The results demonstrated that the sodiation/desodiation of presodiated HC was reversible. Therefore, presodiated HC was selected for further experiments in full-cell fabrication.

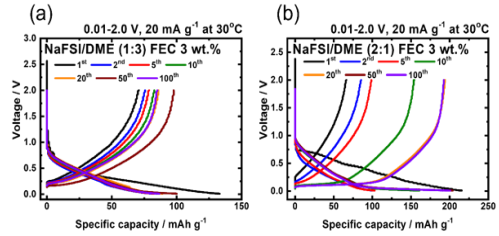

Figure 6. Voltage profiles of pristine HC electrode in (a) dilute and (b) high concentration NaFSI/DME FEC 3 wt.% electrolytes

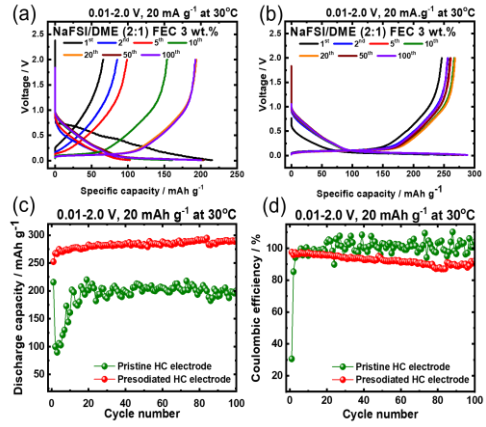

Figure 7. Voltage profiles of (a) pristine and (b) presodiated HC electrodes and cycling performance (c,d) in Na||HC cells

Table 2. Comparison of HC electrodes with and without presodiation in 1st cycle

	Initial charge capacity (mAh g^{-1})	Initial discharge capacity (mAh g^{-1})	Initial Coulombic efficiency (%)
Pristine HC	66.3	215.6	30.6
Presodiation HC	246.3	252.5	97.5

As shown in Figure 8, NVP particles with a size range of 5–15 µm were evenly distributed on Al foil. In full cell configuration, the NVP cathode was coupled with presodiated HC anodes within several N/P ratios, including 0.8, 0.9, 1.0, 1.1, and 1.2, and a glass fiber separator soaked with NaFSI/DME (2:1) FEC 3 wt.%. The cells were cycled in the voltage range 2.5-3.7 V (vs. Na^+/Na) at a current density of C/5. The voltage profiles and cycling performance of HC||NVP full cells were depicted in Figure 9 and Figure 10, respectively. Poor cycling performance was obtained in cells with low N/P ratios of 0.8, and 0.9, which exhibited cell failure at 8th, and 21st cycle, respectively. With three N/P ratios of 1.0, 1.1, and 1.2, the cell with the 1.2 ratio exhibited a dramatic increase in charge capacity, and Coulombic efficiency (CE) dropped to approximately 20% after 50 cycles. In contrast, both the N/P ratios of 1.0 and 1.1 exhibited excellent cycling performance, with the CE remaining at approximately 70% throughout 100 cycles. Specifically, the cells with an N/P ratio of 1.0 provided a sustained discharge capacity of around 90 mAh g^{-1} with a capacity retention of nearly 100% after 100 cycles. Similarly, the cells with an N/P ratio of 1.1 displayed approximately 100 mAh g^{-1} for the first 10 cycles before falling to 81.9 mAh g^{-1} at the 100th cycle, retaining 90.7% of their capacity, as shown in Figure 10 (a). Figure 10 (c) exhibits the effect of N/P ratio on ICE and discharge capacity of as prepared full cells. The ICE, which was an indicator of irreversible capacity or active Na loss in the initial cycle, steadily rose with the increasing N/P, reaching a peak at N/P 1.0 before falling when

N/P was higher than 1.0. At low N/P ratio, when the full cells are charging, the anode potential could close to 0 V (vs. Na^+/Na), the sodium deposition potential, increase sodium plating. A non-homogeneous sodium plating fosters the development of sodium metal dendrites, which can penetrate the separator and induce internal short circuits, ultimately leading to cell failure. A N/P ratio over 1.0 has the potential to inhibit the occurrence of sodium deposition in the anode. An overly elevated N/P ratio may give rise to an overcharging phenomenon inside the cathode electrodes. This can lead to the oxidation of both the electrolytes and cathode materials. The oxidation process contributes to the buildup of the cathode electrolyte interphase (CEI), ultimately resulting in a reduction in capacity.

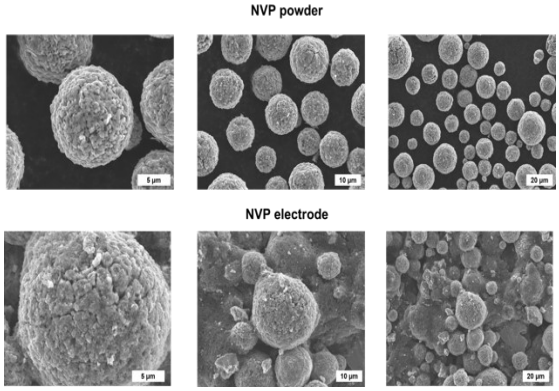

Figure 8. SEM images of NVP powder, and NVP electrodes

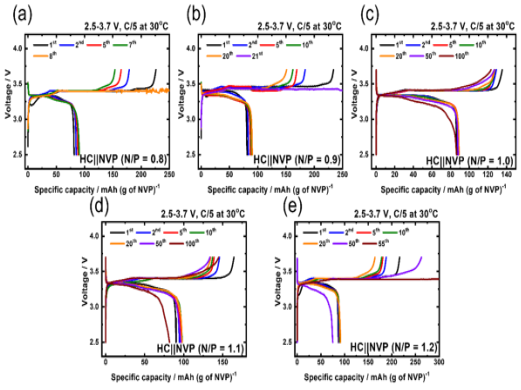

Figure 9. Voltage profiles of HC||NVP full cells with various N/P ratios

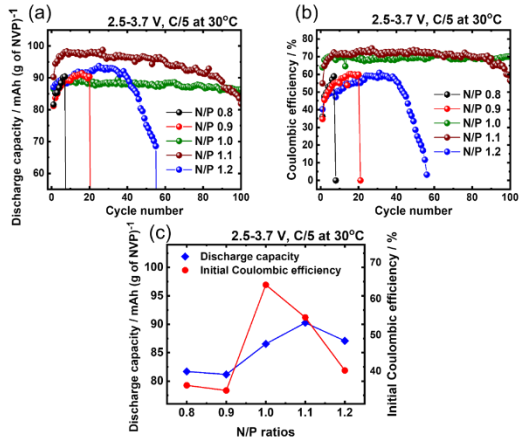

Figure 10. (a,b) Cycling performance, (c) effect of N/P ratios of HC||NVP full cells

To further clarify the reason for cell failure, the cells with various N/P ratios after three formation cycles at C/10 were conducted EIS analysis. The corresponding Nyquist plots as well as the equivalent circuit are shown in Figure 11. The Nyquist plots of all samples comprise two semicircles. The first semicircle is attributed to the resistance of the SEI and CEI layers, while the second one is related to the resistance of the charge transfer process. As seen in Table 3, the $R_{SEI+CEI}$ of the low N/P ratios (0.8 and 0.9) are significantly higher than those of the other N/P ratios (1.0, 1.1, and 1.2). The results could be caused by sodium plating at low N/P ratios. As mentioned above, sodium ions could be transferred to sodium metal on the anode surface at low N/P ratios because the voltage in the anode is close to 0 V (Na+/Na) during battery operation. Furthermore, the inherent high chemical reactivity of Na metal induces decomposition of the electrolyte components upon direct contact. This decomposition process results in the formation of a thicker SEI layer on the anode surface. As shown in Table 3, the RSEI+CEI in those samples grew dramatically poor cycling performance. The excessive N/P ratios could also generate electrolyte oxidation because of the overcharging of the cathode during the operation, which induced the rise of $R_{SEI+CEI}$ and cell failure at the N/P ratio of 1.2 after 50 cycles. However, thanks to the superior electrolyte oxidation stability of high concentration electrolytes (Nguyen et al., 2023), the cells with N/P ratios of 1.0 and 1.1 could avoid electrolyte oxidation in overcharging and maintain excellent cycling performance during 100 cycles.

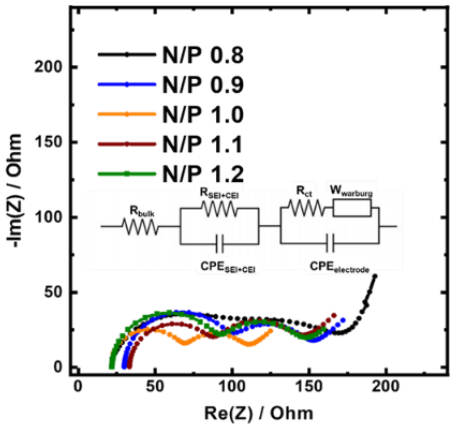

Figure 11. Nyquist plots of HC||NVP full cell after three-cycles formation

Table 3. Resistance of each part in equivalent circuit for HC||NVP cells

N/P ratio	R_{bulk} (Ω)	$R_{SEI+CEI}$ (Ω)	R_{ct} (Ω)
0.8	22.52	83.25	46.68
0.9	29.79	68.4	43.45
1.0	20.61	46.68	34.40
1.1	33.12	47.29	52.61
1.2	21.76	69.15	44.35

4. CONCLUSION

In conclusion, the electrolyte NaFSI/DME (2:1) FEC 3 wt.% could keep preserving its properties at ambient temperature and elevated temperatures (35 °C and 55 °C). With an ICE of 30.6%, the pristine HC anode delivered a discharge capacity of 215.6 mAh g^{-1}. Whereas, based on the simple sodiation method, the sodiated HC anode exhibited 252.5 mAh g^{-1} with an ICE of 97.5% at the first cycle. Full cells comprising an NVP cathode and a sodiated HC anode with a N/P ratio of 1.1 had a discharge capacity of approximately 100 mAh g^{-1} for the initial 10 cycles and a capacity retention of 90.7%, while full cells with a N/P ratio of 1.0 showed a stable discharge capacity of 90 mAh g^{-1} with a capacity retention of nearly 100% after 100 cycles. The cell failure at low or overly high N/P ratios was attributed to SEI and CEI accumulation because of the sodium plating and electrolyte decomposition.

ACKNOWLEDGMENT

This research is funded by University of Science, VNU-HCM under grant number U2022-12.

REFERENCES

Bommier, C., Surta, T. W., Dolgos, M., & Ji, X. (2015). New mechanistic insights on Na-ion storage in nongraphitizable carbon. *Nano Letters*, *15*(9), 5888-5892.

Cao, R., Mishra, K., Li, X., Qian, J., Engelhard, M. H., Bowden, M. E., ... & Zhang, J. G. (2016). Enabling room temperature sodium metal batteries. *Nano Energy*, *30*, 825-830.

Dou, M., Zhang, Y., Wang, J., Zheng, X., Chen, J., Han, B., ... & Cai, Z. (2023). Simultaneous cation-anion regulation of sodium vanadium phosphate cathode materials for high-energy and cycle-stable sodium-ion batteries. *Journal of Power Sources*, *560*, 232709.

Hirsh, H. S., Sayahpour, B., Shen, A., Li, W., Lu, B., Zhao, E., ... & Meng, Y. S. (2021). Role of electrolyte in stabilizing hard carbon as an anode for rechargeable sodium-ion batteries with long cycle life. *Energy Storage Materials*, *42*, 78-87.

Huang, Y., Wang, Y., Bai, P., & Xu, Y. (2021). Storage mechanism of alkali metal ions in the hard carbon anode: an electrochemical viewpoint. *ACS Applied Materials & Interfaces*, *13*(32), 38441-38449.

Hwang, J. Y., Myung, S. T., Choi, J. U., Yoon, C. S., Yashiro, H., & Sun, Y. K. (2017). Resolving the degradation pathways of the O3-type layered oxide cathode surface through the nano-scale aluminum oxide coating for high-energy density sodium-ion batteries. *Journal of Materials Chemistry A*, *5*(45), 23671-23680.

Lee, J., Lee, Y., Lee, J., Lee, S. M., Choi, J. H., Kim, H., ... & Choi, N. S. (2017). Ultraconcentrated sodium bis (fluorosulfonyl) imide-based electrolytes for high-performance sodium metal batteries. *ACS applied Materials and Interfaces*, *9*(4), 3723-3732.

Li, P., Gao, M., Wang, D., Li, Z., Liu, Y., Liu, X., ... & Guo, X. (2023). Optimizing vanadium redox reaction in $Na_3V_2(PO_4)_3$ cathodes for sodium-ion batteries by the synergistic effect of additional electrons from heteroatoms. *ACS Applied Materials & Interfaces*, *15*(7), 9475-9485.

Ma, L., Cui, J., Yao, S., Liu, X., Luo, Y., Shen, X., & Kim, J. K. (2020). Dendrite-free lithium metal and sodium metal batteries. *Energy Storage Materials*, *27*, 522-554.

Moeez, I., Jung, H. G., Lim, H. D., & Chung, K. Y. (2019). Presodiation strategies and their effect on electrode–electrolyte interphases for high-performance electrodes for sodium-ion batteries. *ACS Applied Materials and Interfaces*, *11*(44), 41394-41401.

Nguyen, T. H., & Duong, T. H. N. (2020). Separation and recovery of Co (II) and Li (I) from spent lithium-

ion mobile phone batteries. *Can Tho University Journal of Science*, *12*(2), 60-67.

Nguyen, T. T., Chau, P. Q., Nguyen, N. P. P., Pham, L. T., Nguyen, P. H., Huynh, T. T. K., ... & Van Tran, M. (2023). Synergistic effect of high concentration sodium bis (fluorosulfonyl) imide electrolyte and fluorinated ethylene carbonate enabling stability and high-rate performance of Na metal batteries. *Chemical Physics Letters*, *825*, 140576.

Pan, Y., Zhang, Y., Parimalam, B. S., Nguyen, C. C., Wang, G., & Lucht, B. L. (2017). Investigation of the solid electrolyte interphase on hard carbon electrode for sodium ion batteries. *Journal of Electroanalytical Chemistry*, *799*, 181-186.

Shen, L., Li, Y., Roy, S., Yin, X., Liu, W., Shi, S., ... & Zhao, Y. (2021). A robust carbon coating of $Na_3V_2(PO_4)_3$ cathode material for high performance sodium-ion batteries. *Chinese Chemical Letters*, *32*(11), 3570-3574.

Song, J., Peng, X., Liu, D., Li, H., Wu, M., Fang, K., ... & Tang, H. (2023). On-site conversion reaction enables ion-conducting surface on red phosphorus/carbon anode for durable and fast sodium-ion batteries. *Journal of Energy Chemistry*, *80*, 381-391.

Tran, T. T., Nguyen, V. N. H., Nguyen, T. H., & Lee, M. S. (2023). Investigating the leaching performance of ferric chloride solution for metallic alloys resulting from reduction smelting of spent lithium-ion batteries. *Can Tho University Journal of Science*, *15*(1), 64-70.

Wu, H. M., Belharouak, I., Deng, H., Abouimrane, A., Sun, Y. K., & Amine, K. (2009). Development of $LiNi_{0.5}Mn_{1.5}O_4/Li_4Ti_5O_{12}$ system with long cycle life. *Journal of the electrochemical society*, *156*(12), A1047.

Xiao, L., Lu, H., Fang, Y., Sushko, M. L., Cao, Y., Ai, X., ... & Liu, J. (2018). Low-defect and low-porosity hard carbon with high coulombic efficiency and high capacity for practical sodium ion battery anode. *Advanced Energy Materials*, *8*(20), 1703238.

Xie, F., Xu, Z., Jensen, A. C., Ding, F., Au, H., Feng, J., ... & Titirici, M. M. (2019). Unveiling the role of hydrothermal carbon dots as anodes in sodium-ion batteries with ultrahigh initial coulombic efficiency. *Journal of Materials Chemistry A*, *7*(48), 27567-27575.

Xie, F., Lu, Y., Chen, L., & Hu, Y. S. (2021). Recent Progress in Presodiation Technique for High-Performance Na-Ion Batteries. *Chinese Physics Letters*, *38*(11), 118401.

Yamada, Y. (2020). Concentrated battery electrolytes: Developing new functions by manipulating the coordination states. *Bulletin of the Chemical Society of Japan*, *93*(1), 109-118.

Zhang, L., Deshmukh, J., Hijazi, H., Ye, Z., Johnson, M. B., George, A., ... & Metzger, M. (2023). Impact of Calcium on Air Stability of $Na[Ni_{1/3}Fe_{1/3}Mn_{1/3}]O_2$ Positive Electrode Material for Sodium-ion Batteries. *Journal of The Electrochemical Society*, *170*(7), 070514.

Zheng, J., Chen, S., Zhao, W., Song, J., Engelhard, M. H., & Zhang, J. G. (2018). Extremely stable sodium metal batteries enabled by localized high-concentration electrolytes. *ACS Energy Letters*, *3*(2), 315-321.